

HOSTED BY



ELSEVIER

Contents lists available at ScienceDirect

# Engineering Science and Technology, an International Journal

journal homepage: <http://www.elsevier.com/locate/jestch>

## Full Length Article

# The effect of SiC powder mixing electrical discharge machining on white layer thickness, heat flux and fatigue life of AISI D2 die steel

Ahmed Al-Khazraji <sup>a</sup>, Samir Ali Amin <sup>a</sup>, Saad Mahmood Ali <sup>b,\*</sup><sup>a</sup> Mechanical Engineering Department, University of Technology, District 906 – Alsnaa St., Baghdad, Iraq<sup>b</sup> Mechanical Engineering Department, University of Karbala, Karbala 56001, Iraq

## ARTICLE INFO

### Article history:

Received 5 September 2015

Accepted 23 January 2016

Available online 23 April 2016

### Keywords:

EDM  
PMEDM  
Silicone carbide powder  
RSM  
FEM  
WLT  
Total heat flux  
Fatigue life

## ABSTRACT

This paper deals with studying the effect of powder mixing electrical discharge machining (PMEDM) parameters using copper and graphite electrodes on the white layer thickness (WLT), the total heat flux generated and the fatigue life. Response surface methodology (RSM) was used to plan and design the experimental work matrices for two groups of experiments: for the first EDM group, kerosene dielectric was used alone, whereas the second was treated by adding the SiC micro powders mixing to dielectric fluid (PMEDM). The total heat flux generated and fatigue lives after EDM and PMEDM models were developed by FEM using ANSYS 15.0 software. The graphite electrodes gave a total heat flux higher than copper electrodes by 82.4%, while using the SiC powder and graphite electrodes gave a higher total heat flux than copper electrodes by 91.5%. The lowest WLT values of 5.0  $\mu\text{m}$  and 5.57  $\mu\text{m}$  are reached at a high current and low current with low pulse on time using the copper and graphite electrodes and the SiC powder, respectively. This means that there is an improvement in WLT by 134% and 110%, respectively, when compared with the use of same electrodes and kerosene dielectric alone. The graphite electrodes with PMEDM and SiC powder improved the experimental fatigue safety factor by 7.30% compared with the use of copper electrodes and by 14.61% and 18.61% compared with results using the kerosene dielectric alone with copper and graphite electrodes, respectively.

© 2016 Karabuk University. Publishing services by Elsevier B.V. This is an open access article under the CC BY-NC-ND license (<http://creativecommons.org/licenses/by-nc-nd/4.0/>).

## 1. Introduction

The mixing of a suitable abrasives and metallic material in powder form into the dielectric fluid is one of the latest advancement for improving the innovations and enhancement capabilities of EDM process [1]. This process is called powder mixed EDM (PMEDM). In this process, the electrically conductive powder particles are mixed in the dielectric fluid, which reduces the particles' insulating strength and increase the spark gap distance between the tool and workpiece to spread the electric discharge uniformly in all directions. As a result, the process becomes more stable, thereby improving material removal rate (MRR) and surface finish [2,3].

Razak et al. [4] conducted investigations on powder concentration and powder particles size of silicon carbide PMEDM based on

Taguchi orthogonal array. The outcomes are expected to be capable of increasing MRR, improving surface finish, reducing TWR, and reducing machining time and cost.

EDM is a thermal erosion process [5]. Instantaneous temperature rise during the machining process changes the physical properties of the machining surface layer, resulting in the presence of residual stress, which is one of the key factors affecting the machined surface quality and its functional performance.

Abhijeetsinh and Kapil [6] studied the influence of process parameters and electrode shape configuration on AISI 316 Stainless steel workpiece material and pure copper as electrode material. Detailed analysis of structural features of machined surface is done by using Scanning Electron Microscope (SEM) to understand the mode of heat affected zone (HAZ), recast layer thickness and micro cracks, which alternatively affects structure of machined workpiece and hence tool life.

The high magnitude thermal residual stresses, which are created on the upper layer of workpiece surface due to rapid solidification of EDM processes, influence the component properties. They increase with increasing pulse energy [7,8]. EDM components are commonly applied in high temperature, high-stress, and high-fatigue-load environments. Under such conditions, the cracks on the machined surface act as stress raisers and lead to a considerable

The authors confirm that this work has not been published previously (except as part of academic thesis), that it is not under consideration for publication elsewhere, that its publication is approved by all authors and that it will not be published elsewhere in the same form, in English or in any other language, without the written consent of the Publisher.

Peer review under responsibility of Karabuk University.

\* Corresponding author. Tel.: +96 478 03700877.

E-mail address: [smaengg@yahoo.com](mailto:smaengg@yahoo.com) (S.M. Ali).

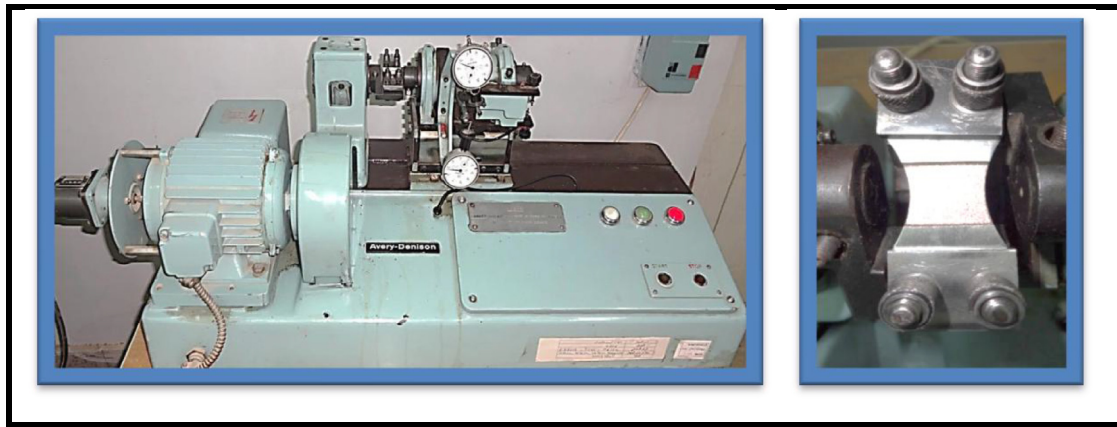


Fig. 1. The Avery Denison plain bending fatigue testing machine type 7305, England.

reduction in the fatigue life of the component. Accordingly, the current study conducts an experimental investigation of the powder mixing method, which does not require post-treatment processing to identify the optimal EDM machining parameters that suppress the formation of cracks in the recast layer for longest lives under different fatigue loads.

Mehdi et al. [9] used Response surface methodology (RSM) to analyze the effect of EDM input parameters for machining Al–Mg 2Si composite material on microstructure changes. The results show that voltage and current, and pulse on time are the most significant factors on microstructure of machined surfaced.

A considerable amount of work has been reported by the researchers on the measurement of EDM performance on the performance parameters with various DOE and optimization techniques especially utilizing the Response surface methodology [10–15].

The objective of this study concerns the effects of SiC powder mixing (PMEDM) parameters on the total heat flux generated, white layer thickness (WLT) and fatigue life properties of the selected AISI die steel workpiece, and developing numerical models for verifying the experimental results by using the response surface methodology (RSM) and the finite element method (FEM) with ANSYS 15.0 software.

The adoption of the current work goals were intended within other targets to reach the best combination parameters because this type of die and mold steel owns its global importance in engineering industries as well as the significance of EDM processes.

## 2. Experimental work

The workpiece material was prepared for chemical composition, mechanical properties tests and Rockwell hardness tests on the bases of ASTM-77 steel standard for mechanical testing of steel products [16]. The workpiece specimens were prepared with dimensions  $89.9 \times 30 \times 4.25$  mm, according to requirement of the Avery type 7305 plain bending fatigue testing machine, as shown in Fig. 1.

The average values of chemical composition of the selected workpiece material and the equivalent values given according to ASTM A 681-76 standard specification for alloy and die steels [17]

are listed in Table 1. The results of tensile test and Rockwell hardness tests are given in Table 2. The chemical composition of the copper electrodes are listed in Table 3. The used kerosene dielectric was tested according to the ASTM (D 3699-90) industry standard specifications for kerosene. The chemical composition of the silicon carbide powder was tested for compositions by using the X-ray diffraction tester.

Two types of electrode materials were selected (Copper and Graphite) with dimension of  $30 \times 24 \times 24$  mm. The copper electrode material was examined for chemical composition properties using the X-Met 3000TX HORIZONTAL metal analyzer. Both selected electrode materials have their own extensive industrial applications. Copper is more widely used, while graphite is also used in industrial and researches areas. The current work will attempt to prove the high role of graphite in improving the performance responses of the process. There are other electrode materials used, but with less applications, like aluminum and even steels.

SiC powder was chosen as a mixed powder with kerosene dielectric because it has many important properties such as high melting point, strength and electrical resistivity. The average grain size for silicon carbide powder is  $95.502 \mu\text{m}$ .

The powder with this particle size has been used to increase the micro shooting effect of its solid particles and consequently increases the material removal rates, and improves surface residual stresses and other properties of machined workpiece in addition to the cheapness price, which makes the process of mixing very suitable in economic terms.

The EDM parameters are: the gap voltage  $V_p$  (140 V), the pulse on time duration period  $T_{on}$  (40 and 120  $\mu\text{s}$ ), the pulse off time duration period  $T_{off}$  (14 and 40  $\mu\text{s}$ ), the pulse current  $I_p$  (8 and 22 A), the duty factor ( $\eta = 75\%$ ), two sides flashing pressure = 0.73 bar (10.3 psi.) and the SiC powder mixing concentration (0 and 5 g/L).

In this work, for optimum machining performance measures, selecting the proper combination of machining parameters is an important task. Generally, the machining parameters were selected on the basis of data provided by the EDM manufactures and research works. Such data were not available for the AISI D2 die steel, especially when using the graphite electrodes, the SiC and graphite mixing powder.

Table 1  
The chemical compositions of workpiece material.

Sample	C %	Si %	Mn %	P %	S %	Cr %	Mo %	Ni %	Co %	Cu %	V %	Fe %
Tested (Average)	1.51	0.174	0.264	0.014	0.003	12.71	0.555	0.158	0.0137	0.099	0.306	Bal.
Standard AISI D2	1.40 to 1.60	0.60 max.	0.60 max.	0.03 max.	0.03 max.	11.00 to 3.00	0.70 to 1.20	–	1.00 Max.	–	1.10 Max.	Bal.

**Table 2**  
The mechanical properties of the selected materials.

Sample	Ultimate tensile stress N/mm <sup>2</sup>	Yield strength N/mm <sup>2</sup>	Elongation %	Hardness HRB
Average	704.25	415.25	18.125	90.75

In this work, the analytical and statistical response surface methodology (RSM) method was used to select best combination of process parameters for an optimum machining performance and giving the best design of experiment DOE matrix with minimum numbers of experiments. RSM analyze the experimental data by plotting Interaction graphs, residual plots for accuracy and response curves [12]. A Box–Behnken design as a type of response surface design was used, which does not contain an embedded factorial or fractional factorial design to determine the best responses conditions.

For the purpose of powder mixing with dielectric fluid (PMEDM), a stainless steel container (of about 30 liters volume and overall dimensions of 400 × 300 × 230 mm with a cover of 400 × 230 mm and 3 mm thickness) was fabricated, which contained kerosene dielectric pump, an electric motor (300 RPM) connected to a mixer and stainless steel impellers, a workpiece clamping fixture, valves and pipe accessories. For the power supply, an AC/DC converter for driving the special kerosene pump was installed in an electrical board made especially for this work. This board contained also a pressure gauge (one bar capacity) as shown in Fig. 2.

In this work, two groups were planned, each containing 22 experiments using a new set of workpiece and electrode in each experiment. The first 11 experiments in each group were machined by using the copper electrodes, while the last 11 experiments were done by using the graphite electrodes. The specimens after EDM machining with the used copper and graphite electrodes for both groups are shown in Fig. 3.

For studying of the influence of EDM parameters and electrode material types on the surface recast white layers micro defects, the optical stereo microscope (OSM) was used. The selected specimens were prepared after grinding, polishing and etching processes

for surface topography examination. The white layer thickness (WLT) inspections were implemented by using the Optical microscope (OM).

**3. Modeling and simulation of the heat flux using FEM**

Due to the random, high complexity and uncertainty nature of EDM, the following assumptions have been considered to make the problem mathematically feasible for all proposed EDM and PMEDM models unless otherwise specified:

- 1 An axisymmetric model has been considered.
- 2 Workpiece materials are homogeneous and isotropic in nature [18].
- 3 The material properties of the workpiece and tool are temperature dependent.
- 4 Density and element shape are not affected [19].
- 5 EDM discharge spark channel is considered as a uniform cylindrical column shape.
- 6 The heat source is assumed to have Gaussian distribution of heat flux on the surface of the workpiece material during pulse on time period [20,21].
- 7 Temperature analysis is considered to be of transient type [18,22].
- 8 The channel diameter is approximately between 10 μm and 100 μm, thus the electrode can be considered as a semi-infinite body.
- 9 The magnitude of the heat flux incident on the electrodes is independent of the affected surface profile.

Many authors have considered uniformly distributed and the hemi-spherical disc heat source within a spark [23,24]. This assumption is far from reality for thermal modeling in EDM. However, Dibitonto et al. [20], Eubank et al. [25] and Bhattacharya et al. [26] have shown that the Gaussian heat distribution is more realistic than disc heat source for modeling the heat input in EDM. This fact is evidenced from the actual shape of a crater formed during EDM.

**Table 3**  
The chemical compositions of copper electrodes material.

Zn %	Pb %	Si %	Mn %	P %	S %	Sn %	Al %	Ni %	Sb %	Fe %	Cu %
0.006	0.001	0.011	0.0002	0.005	0.002	0.0005	0.007	0.004	0.005	0.007	99.96



**Fig. 2.** The (CNC) EDM machine with all the fabricated accessories.

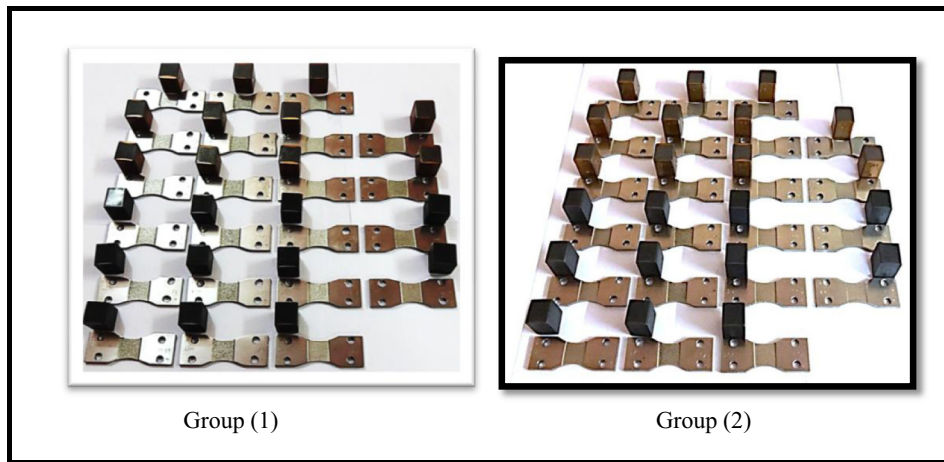


Fig. 3. The specimens and the used copper and graphite electrodes for groups (1 and 2) experiments after EDM and PMEDM machining.

The intensity of heat imparted to the workpiece surface, which is denoted by  $Q_w$ , is a function of instantaneous spark radius ( $r$ ). The Gaussian distribution of heat applied at the axis of a spark for a single discharge with a maximum radius ( $R$ ), and then the heat flux  $Q_w(r)$  at radius  $r$  of the system is given by the following relation [18]:

$$Q_w(r) = \frac{4.57 * R_w * V_b * I_p * Kn}{\pi * R^2} e^{-4.5 \frac{r^2}{R^2}} \quad (1)$$

The rate of energy incident on the workpiece is equal to the rate of energy supplied, which is equal to  $R_w * V_p * I_p$ , where  $R_w$  is the energy percentage fraction of heat input to the workpiece,  $V_b$  is the breakdown voltage (different from the applied voltage),  $R$  is the spark radius in  $\mu\text{m}$ , and  $I_p$  is the discharge current.

The value of  $R_w$  has been determined by Shuvra et al. [19], Dibitonto et al. [20] and Patel et al. [21] who have suggested that a constant fraction of the total power is transferred to the electrodes. They have used the value of  $R_w$  as 8% as the percentage of heat input absorbed by the workpiece for their theoretical work of conventional EDM, and the same value was used in this work. The  $R_w$  values during PMEDM in the present model have been assumed to be 9% of the total heat lost in the workpiece. Shankar et al. [22] have calculated that about 18% is absorbed by the cathode and the rest is discharged to the dielectric fluid.

The breakdown voltage value ( $V_b$ ) is taken as 20 V, while for PMEDM it is about 20%–30% lower than that for EDM, i.e.,  $V_b = 15$  V. The spark radius ( $R$ ) was taken as 15  $\mu\text{m}$ , and the heat flux for AISI D2 die steel is  $Q_w(r) = 680 \text{ MW/m}^2\text{K}$  for various values of discharge current. The spark radii for PMEDM processes were taken to be 40% larger than traditional EDM.

The new parameter ( $Kn$ ), which takes into account the effect of suspended powder particles on the spark frequency and breakdown voltage, was also calculated. The value of  $Kn$  depends upon the type of powder and the powder properties, such as shape, size, concentration etc. The values of  $Kn$  factor were experimentally estimated for EDM and PMEDM machining groups as given in Table 4 using the results of material removal rates which were experimentally calculated.

Marafona and Chousal [27] suggested an equation called the equivalent heat input radius  $R(t)$  or the radius of plasma channel ( $\mu\text{m}$ ), which is dependent on the current intensity ( $I_p$ ) and pulse on duration ( $T_{on}$ ), thereby:

$$R(t) = 2.04 * I_p^{0.43} * T_{on}^{0.44} \quad (2)$$

The total heat flux generated and absorbed by the workpiece, electrode and dielectric can be calculated for machining area is about 500  $\text{mm}^2$  and the effective geometric machining area is about 0.75% of the above total machining area and about 10% of the total numbers of discharge sparks generated instantaneously during one pulse on period of time, then:

$$\begin{aligned} \text{The total number of discharge sparks (SN)} & \quad (3) \\ & = \text{Total machining area} \times 20\% \times 0.75 / \text{Area of one discharge spark} \end{aligned}$$

The total heat fluxes for all EDM experiments were calculated using equation (1), but this equation needs to modify as:

$$Q_w(r) = \frac{4.57 * R_w * V_b * I_p * Kn}{\pi * R^2} e^{-4.5 \frac{r^2}{R^2}} \times \text{SN} / \text{Machining area of the workpiece} \quad (4)$$

Table 4

The average values of material removal rate (MRR) and the experimentally estimated values of  $Kn$  factor for all EDM and PMEDM machining groups.

Exp. no.	Type of electrode	Pulse on time $T_{on}$ ( $\mu\text{s}$ )	Pulse off time $T_{off}$ ( $\mu\text{s}$ )	Pulse current (A)	Material removal rate – average values (MRR) $\text{mm}^3/\text{min}$		Average values of $Kn$ coefficient	
					Group 1 Av.	Group 2 Av.	Group 1	Group 2
1.	Copper	120	40	8	8.6789	19.6368	1.00	5.05
2.	Copper	120	40	22	27.2888	40.7208	1.00	3.42
3.	Copper	40	14	8	7.6445	12.2038	1.00	4.16
4.	Copper	40	14	22	16.4341	32.7842	1.00	4.79
5.	Graphite	120	40	8	7.0185	26.2421	0.75	9.02
6.	Graphite	120	40	22	34.4913	71.0767	1.40	4.47
7.	Graphite	40	14	8	9.7517	12.3534	1.24	3.40
8.	Graphite	40	14	22	24.7480	65.2185	1.82	5.26

**Table 5**

The total heat flux fraction values absorbed by the workpieces, the electrodes and kerosene dielectric for group (2).

Exp. no.	Type of electrode	Pulse on duration $T_{on}$ ( $\mu$ s)	Pulse off duration $T_{off}$ ( $\mu$ s)	Pulse current (A)	Heat flux percentage fraction absorbed by the [MW/m <sup>2</sup> ]		
					Workpiece	Electrode	Kerosene dielectric
1.	Copper	120	40	8	157.40	354.15	1437.06
2.	Copper	120	40	22	122.82	276.35	1121.35
3.	Copper	40	14	8	342.26	770.09	3124.83
4.	Copper	40	14	22	451.54	1015.97	4122.56
5.	Graphite	120	40	8	210.88	474.48	1925.33
6.	Graphite	120	40	22	277.56	624.51	2534.12
7.	Graphite	40	14	8	346.88	780.48	3167.01
8.	Graphite	40	14	22	902.45	2030.51	8239.37

The results for the total heat fluxes entering the workpiece, the electrode and the dielectric fluid during the on-time for all PMEDM experiments are given in Table 5. The theoretical and numerical total heat flux generated by the using copper and graphite electrodes and FEM and ANSYS solutions for experimental group (2) is given in Table 6. The percentage increase in the value of the experimental total heat flux using SiC mixed powder (group 2) compared with that in group (1) using kerosene dielectric alone is given in Table 7.

The maximum total heat flux generated by the discharge processes and obtained by the FEM and ANSYS solutions and simulations after EDM machining using copper and graphite electrodes for group (2) are given in Fig. 4. In the present study, a three-dimensional axisymmetric model is developed to predict the total heat flux in AISI D2 die steel workpiece using the transient thermal FE Analysis ANSYS software.

The three-dimensional meshed domain models of the workpiece, the electrode and the used kerosene dielectric were done by using the mapped meshing technique with a triangle element pattern shape with more elements mapped toward the heat-affected regions for better study. The total elements and nodes numbers are 54,407 and 46,664, respectively. The numbers of contact elements are 31,444 and the solid elements are 22,963. The smoothness of

elements is of medium size and their minimum edge length is  $2.51 \times 10^{-3}$  m.

Fig. 4 shows two simulations models for maximum values of input EDM parameters using copper and graphite electrodes, respectively. The right figures represent the total heat flux generated form of the electrode, the workpiece and the kerosene dielectric after hiding the stainless steel container. The figures in the left show the thermal model of the electrode and workpiece after the hiding of kerosene dielectric with the values of maximum heat flux generated and the input EDM and PMEDM processes parameters and also the verified percentage errors between the experimental thermal models compared with the theoretical calculations.

Three levels factorial response surface methodology (RSM) and the Design-Expert 9.0 software were used to analyze the obtained total heat power for each parametric subgroup, the analysis of results for both experimental groups using copper and graphite electrodes are shown in Figs. 5 and 6.

The Model F-value of 31,212.03 implies that the model is significant. The “Pred R-Squared” of 0.9997 is in reasonable agreement with the “Adj R-Squared” of 1.0000; i.e. the difference is less than 0.2.

The predicted equation of the total heat flux generated for PMEDM experimental group (2), using copper electrodes and kerosene dielectric with SiC powder mixing, is:

**Table 6**

The experimental and numerical total heat flux (power) generated by PMEDM processes using kerosene dielectric with SiC mixed powder.

Exp. no.	Type of electrode	Pulse on time $T_{on}$ ( $\mu$ s)	Pulse off time $T_{off}$ ( $\mu$ s)	Pulse current (A)	Experimental total heat flux [MW/m <sup>2</sup> ]	Numerical total heat flux [MW/m <sup>2</sup> ]	Error in numerical mode %
1.	Copper	120	40	8	1948.61	2026.60	+4.0
2.	Copper	120	40	22	1520.52	1579.90	+3.9
3.	Copper	40	14	8	4237.18	4414.70	+4.2
4.	Copper	40	14	22	5590.07	5826.60	+4.2
5.	Graphite	120	40	8	2610.69	2374.30	-9.0
6.	Graphite	120	40	22	3436.19	3118.00	-9.3
7.	Graphite	40	14	8	4294.37	3891.10	-9.3
8.	Graphite	40	14	22	11,172.33	10,087.00	-9.7

**Table 7**

The experimental heat flux (power) generated by EDM (group 1) and PMEDM (group 2) processes.

Exp. no.	Type of electrode	Pulse on time $T_{on}$ ( $\mu$ s)	Pulse off time $T_{off}$ ( $\mu$ s)	Pulse current (A)	Experimental total heat flux [MW/m <sup>2</sup> ]		Percentage increase in total heat flux (%)
					Group (1)	Group (2)	
1.	Copper	120	40	8	434.62	1948.61	+348.4
2.	Copper	120	40	22	531.88	1520.52	+185.9
3.	Copper	40	14	8	1218.50	4237.18	+247.7
4.	Copper	40	14	22	1396.12	5590.07	+300.4
5.	Graphite	120	40	8	346.26	2610.69	+654.0
6.	Graphite	120	40	22	919.62	3436.19	+273.7
7.	Graphite	40	14	8	1511.00	4294.37	+184.2
8.	Graphite	40	14	22	2541.00	11,172.33	+339.7

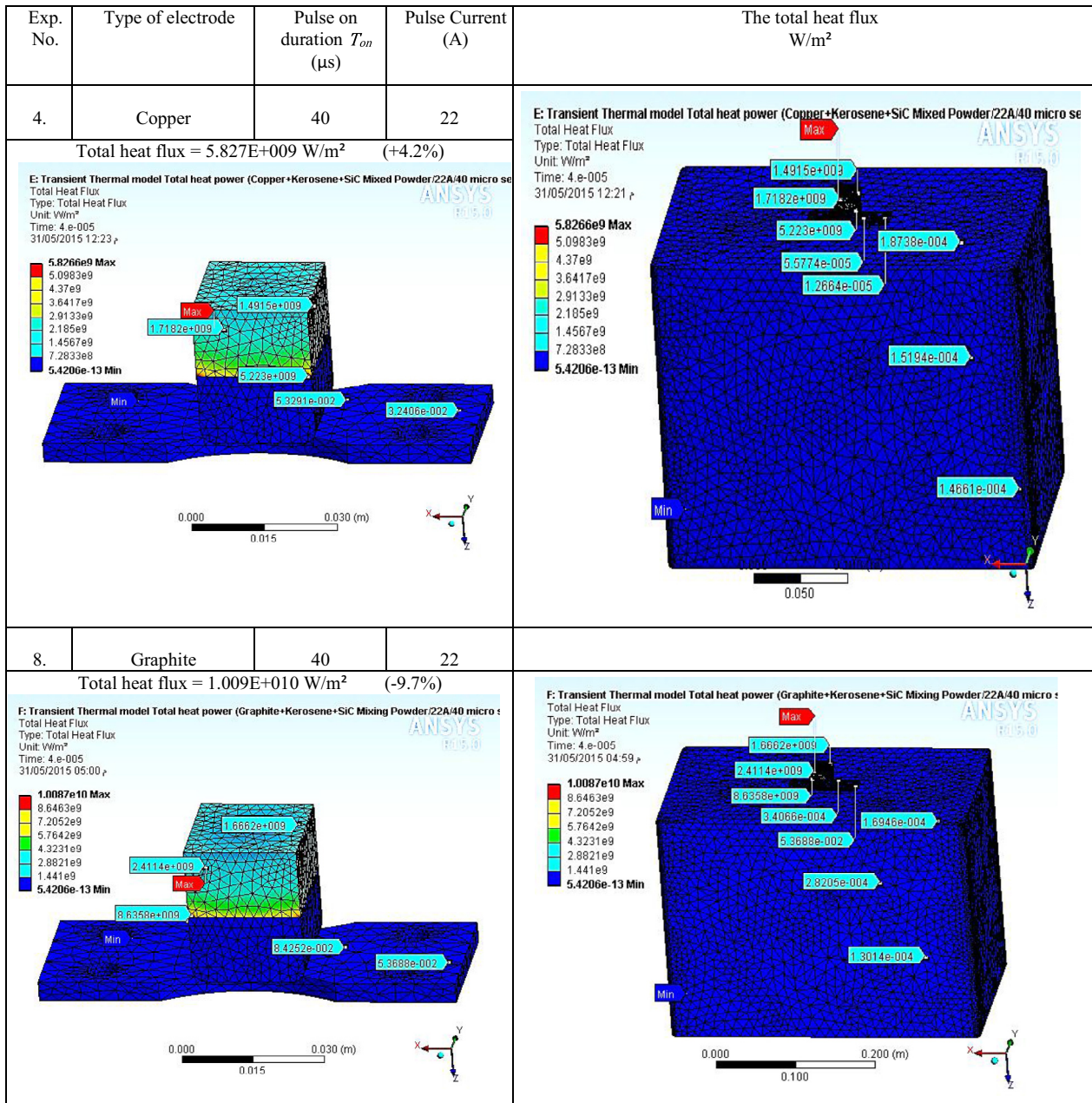


Fig. 4. The total modeled heat flux generated by the PMEDM experiments using the SiC powder, the pulse current (22 A) and the pulse on time (40  $\mu$ s).

$$\text{Total heat power} = +4986.48607 + 125.03143 * \text{Pulse current} - 44.22331 * \text{Pulse on time } (T_{on}) \quad (5)$$

And, using graphite electrodes, the equation is:

$$\text{Total heat power} = +7447.41107 + 125.03143 * \text{Pulse current} - 44.22331 * \text{Pulse on time } (T_{on}) \quad (6)$$

The total heat flux generated by the discharge processes for experimental group (2), using the copper electrodes and SiC mixed powder reached the maximum value as  $5.827 * 10^9$   $W/m^2$  at a pulse current value of 22 A and a pulse on time of 40  $\mu$ s. While, when using graphite electrodes, the total heat flux values reached the maximum value as  $1.009 * 10^{10}$   $W/m^2$  at the same input current and time on period.

This means that the use of graphite electrodes and the kerosene dielectric with SiC mixed powder yields higher total heat flux values by 91.5% when compared with the use of copper electrodes and by 285.3% and 602.7% more when using copper and graphite electrodes and the kerosene dielectric alone, respectively.

The high total heat flux levels are obtained when using the graphite electrodes and the SiC mixed powder as both own low thermal and electrical conductivity and high electrical resistivity compared with copper electrodes. Therefore, when high pulse current passage through the gap between the electrode and the workpiece, a plasma channel with high thermal energy is generated, but cannot able to transform them into fusion state, because of the high melting points of both materials. Then this plasma channel moves to the surface of the workpiece and starts the main effect of the abrasive powder working on enlarged the electrodes gaps and give more

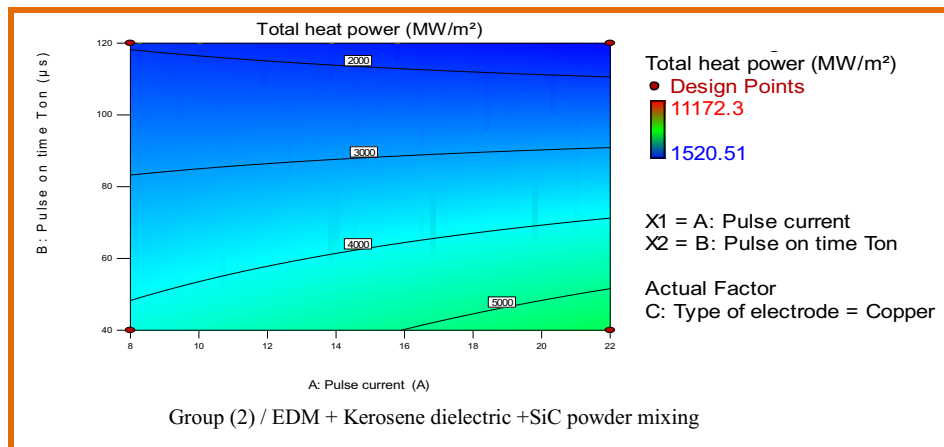


Fig. 5. The total heat flux (power) generated by the EDM machining using copper electrodes and SiC powder mixing.

arranged discharge plasma channels consequentially an increase in the amount of metal removal rate were caused by increase of the melting and eroded areas within the heating periods.

4. Calculation of the white layer thickness (WLT)

The average of three values of workpieces WLT measurements after EDM machining for both experimental groups using the two groups is given in Table 8.

The Model F-value of 7.33 implies that the model is significant. The “Pred R-Squared” of 0.9998 is in reasonable agreement with the “Adj R-Squared” of 1.0000; i.e. the difference is less than 0.2. The

predicted equation of WLT for EDM machining using copper electrodes and SiC mixed powder obtained from using the three levels factorial response surface methodology (RSM) and the Design-Expert 9.0 software is:

$$WLT = +4.40179 + 0.023214 * \text{Pulse current} + 0.055125 * \text{Pulse on time } (T_{on}) \tag{7}$$

And, for graphite electrodes, the equation is:

$$WLT = +5.17679 + 0.023214 * \text{Pulse current} + 0.055125 * \text{Pulse on time } (T_{on}) \tag{8}$$

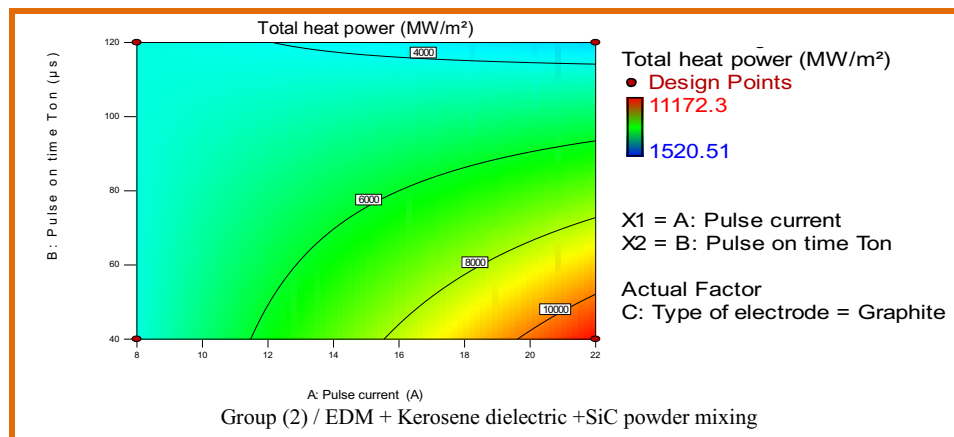


Fig. 6. The total heat flux (power) generated by the EDM using graphite electrodes and SiC powder mixing.

Table 8 Calculation the average values of the white layer thickness (WLT) after EDM and PMEDM machining.

Exp. no.	Type of electrode	Pulse on $T_{on}$ (µs)	Pulse off $T_{off}$ (µs)	Pulse current (A)	Average WLT Group (1) (µm)	Average WLT Group (2) (µm)
1.	Copper	120	40	8	33.34	8.90
2.	Copper	120	40	22	26.67	13.34
3.	Copper	40	14	8	13.34	9.40
4.	Copper	40	14	22	11.67	5.00
5.	Graphite	120	40	8	20.00	13.67
6.	Graphite	120	40	22	8.34	11.10
7.	Graphite	40	14	8	15.00	5.57
8.	Graphite	40	14	22	15.00	9.40

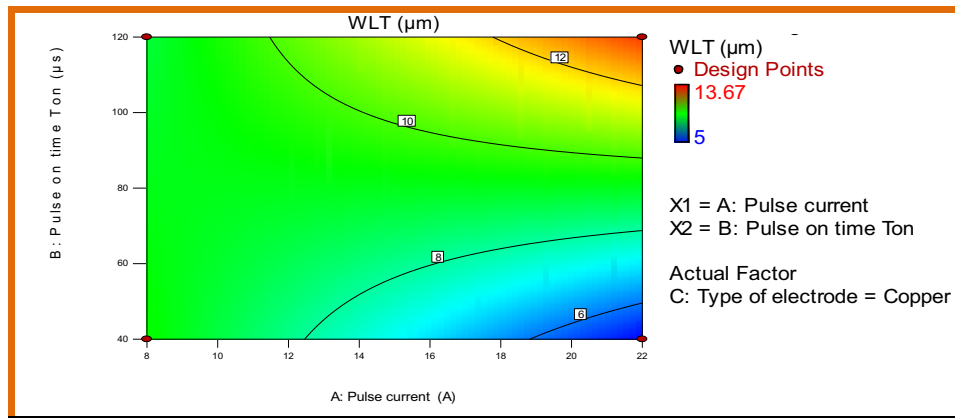


Fig. 7. The WLT for experimental group (2) after PMEDM using copper electrodes.

The average of WLT for after PMEDM machining using the copper and graphite electrodes is shown in Figs. 7 and 8, respectively. For experimental group (2) using the SiC mixed powder and copper electrodes, the WLT reached the minimum value as 5.0  $\mu\text{m}$  at a current value of 22 A and a pulse time of 40  $\mu\text{s}$ , whereas when using the graphite electrodes, the WLT reached the minimum value as 5.57  $\mu\text{m}$  at the input current 8 A and with the same time on a period of 40  $\mu\text{s}$ . This means that there is improvement by 134% and 67% when compared with using of copper and graphite electrodes, and using kerosene dielectric alone, respectively.

The lower levels of the obtained WLT when using the copper electrodes and the abrasive SiC have high hardness work on removal of the melted white layer at high rates by micro shot peening process with a short period of time on/off and then with high pulse current. This is because a high sparks heat power produced with a good arrangements of the plasma channels and the use of dielectric flushing from the both sides of cutting zone. The micro shot peening process required a longer period of time when using the graphite electrodes because, they producing a lower discharge heat power.

The images in Tables 9 and 10 show the macro graphic and microstructure of the heat affected zones (HAZ) for the workpieces surfaces for each subgroup input parameters after EDM and PMEDM processes (groups 1 and 2) using copper and graphite electrodes. These images reveal that the craters sizes increased with the increase in the pulse current and the time on duration, and they reached their minimum sizes, especially when using the graphite

electrodes where higher plasma discharge heat power was generated.

The construction of these microscopic layers and HAZ for experimental group (2) indicates that lower layer thicknesses and defects exist due to the high abrasive and micro shot peening properties of the silicon carbide powder and the plasma discharge pressure of the process as well as the high role of the dielectric flushing of the formed craters from both sides of the cutting areas. With high pulse current value and time on duration, the defects sizes were increased in these layers, especially when using the copper electrodes due to the high thermal energy generated. These figures show the discontinuity and uncompleted formation of the white recast layer, especially when using the copper electrodes due to the high heat power produced and the abrasive properties of the SiC powder materials.

## 5. Modeling and simulation of the fatigue life using FEM

In the present work, the three-dimensional analysis and modeling for EDM of AISI D2 die steel was studied. The damage model was developed to study the influence of different parameters on the workpiece fatigue life. The objective of fatigue analysis is to explain the characterizing capability of a material component to serve the designed cycles loads during its lifetime [28].

The main assumptions of the models are as showing below:

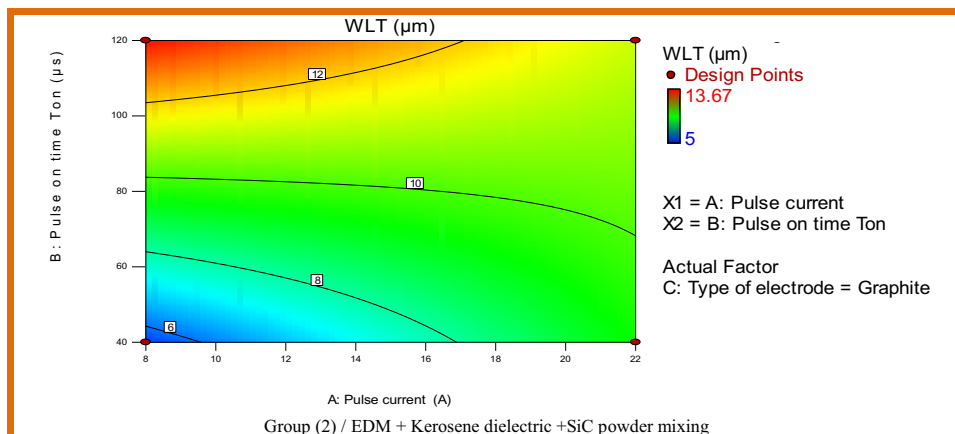
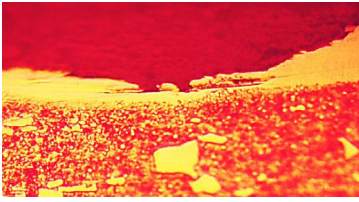
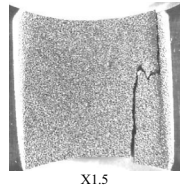
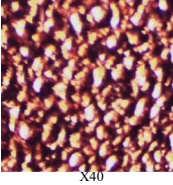
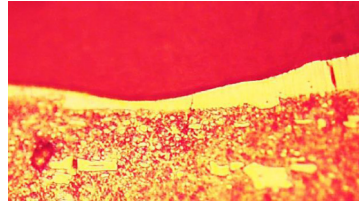
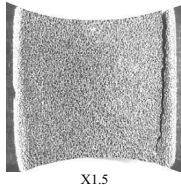
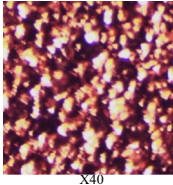
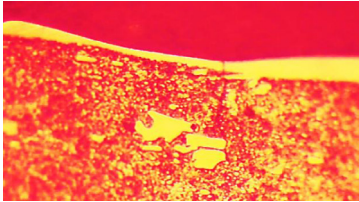
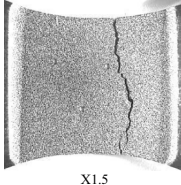
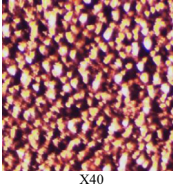
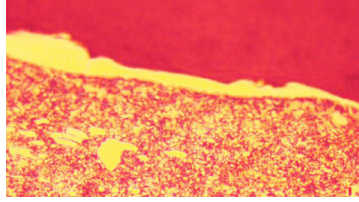
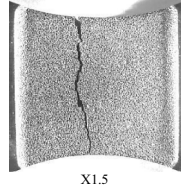
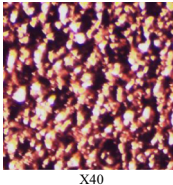
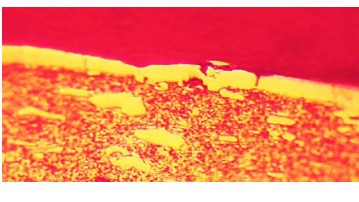
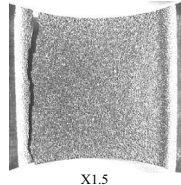
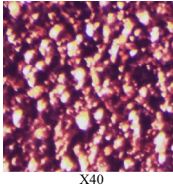
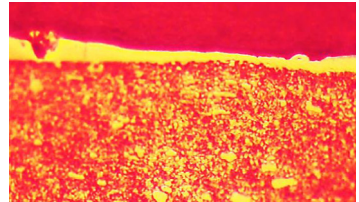
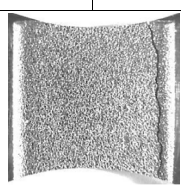
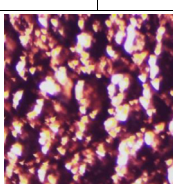
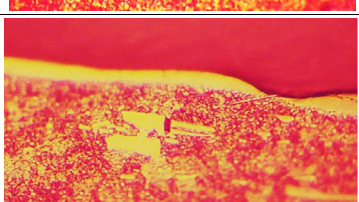
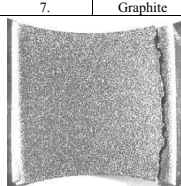
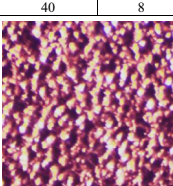
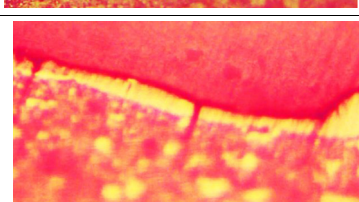
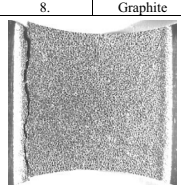
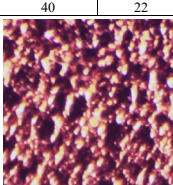
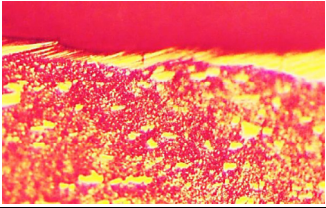
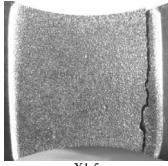
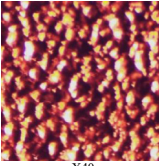
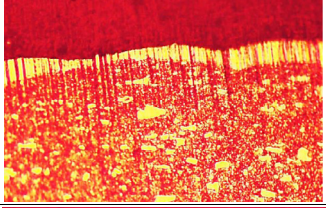
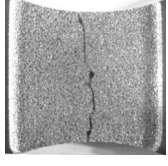
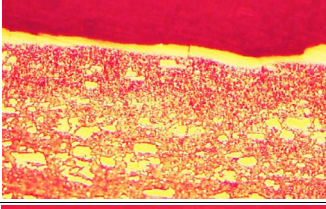
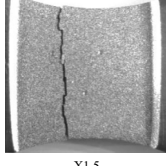
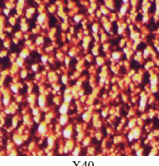
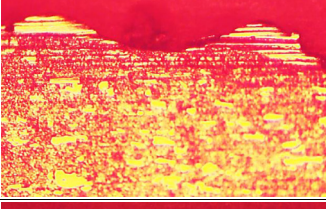
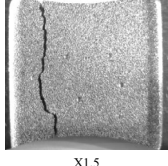
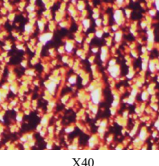
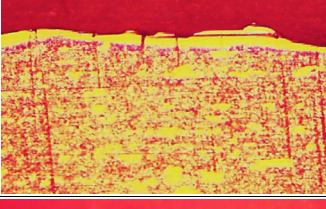
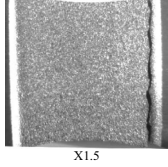
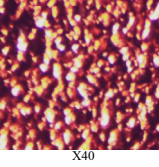
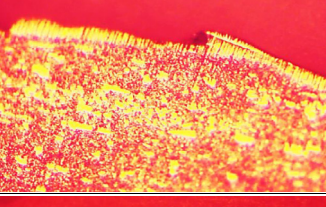
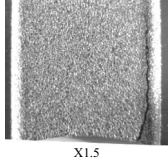
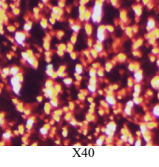
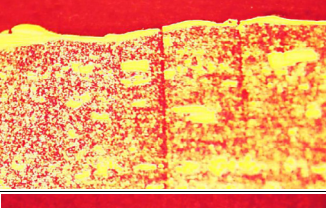
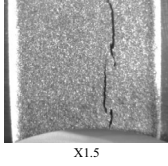
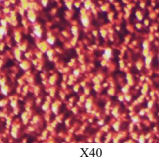
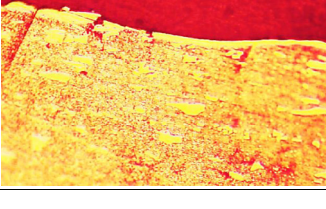
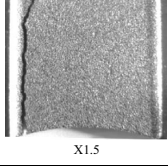
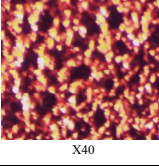


Fig. 8. The WLT for experimental group (2) after PMEDM using graphite electrodes.

**Table 9**  
The white layer thickness (WLT) and HAZ microstructures for EDM group (1) using kerosene dielectric alone.

Exp. No.	Type of electrode	Pulse on duration Ton (μs)	Pulse Current (A)	The white layer microstructure (optical microscope X300)
1.	Copper	120	8	
		 X1.5	 X40	
2.	Copper	120	22	
		 X1.5	 X40	
3.	Copper	40	8	
		 X1.5	 X40	
4.	Copper	40	22	
		 X1.5	 X40	
5.	Graphite	120	8	
		 X1.5	 X40	
6.	Graphite	120	22	
		 X1.5	 X40	
7.	Graphite	40	8	
		 X1.5	 X40	
8.	Graphite	40	22	
		 X1.5	 X40	

**Table 10**  
The WLT and HAZ microstructures for PMEDM group (2) using kerosene dielectric and SiC mixed powder.

Exp. No.	Type of electrode	Pulse on duration $T_{on}$ ( $\mu$ s)	Pulse Current (A)	The white layer microstructure (optical microscope X300)
1.	Copper	120	8	
	 X1.5	 X40		
2.	Copper	120	22	
	 X1.5	 X40		
3.	Copper	40	8	
	 X1.5	 X40		
4.	Copper	40	22	
	 X1.5	 X40		
5.	Graphite	120	8	
	 X1.5	 X40		
6.	Graphite	120	22	
	 X1.5	 X40		
7.	Graphite	40	8	
	 X1.5	 X40		
8.	Graphite	40	22	
	 X1.5	 X40		

**Table 11**

The experimental fatigue life results after EDM and PMEDM machining.

Exp. no.	Type of electrode	Pulse on time $T_{on}$ ( $\mu$ s)	Pulse current (A)	Pulse off time $T_{off}$ ( $\mu$ s)	For group (1)		For group (2)	
					Applied stress ( $\sigma$ ) (MPa)	No. of cycles to failure ( $\times 1000$ )	Applied stress ( $\sigma$ ) (MPa)	No. of cycles to failure ( $\times 1000$ )
1.	Copper	120	8	40	350.00	100.250	350.00	138.250
2.	Copper	120	8	40	300.00	239.750	300.00	304.000
3.	Copper	120	8	40	230.00	1260.500	250.00	1225.000
4.	Copper	120	22	40	350.00	61.000	350.00	85.500
5.	Copper	120	22	40	300.00	133.500	300.00	188.000
6.	Copper	120	22	40	215.00	1273.250	230.00	1304.000
7.	Copper	40	8	14	350.00	84.250	350.00	125.750
8.	Copper	40	8	14	300.00	199.750	300.00	264.250
9.	Copper	40	8	14	220.00	1157.500	240.00	1207.000
10.	Copper	40	22	14	350.00	56.250	350.00	74.000
11.	Copper	40	22	14	210.00	1212.500	220.00	1196.250
12.	Graphite	120	8	40	350.00	94.500	350.00	183.500
13.	Graphite	120	8	40	300.00	214.750	300.00	436.250
14.	Graphite	120	8	40	220.00	1319.000	270.00	1164.000
15.	Graphite	120	22	40	350.00	45.250	350.00	113.250
16.	Graphite	120	22	40	300.00	87.250	300.00	258.750
17.	Graphite	120	22	40	200.00	1063.750	250.00	1226.000
18.	Graphite	40	8	14	350.00	70.250	350.00	154.000
19.	Graphite	40	8	14	300.00	164.750	300.00	352.250
20.	Graphite	40	8	14	215.00	1201.500	260.00	1263.500
21.	Graphite	40	22	14	350.00	51.250	350.00	106.000
22.	Graphite	40	22	14	200.00	1188.500	240.00	1271.500

- 1 The EDM and PMEDM damaged layers cannot carry any load cycles during fatigue. Therefore, the fatigue damage begins beneath the damaged layer, not at the top surface of the specimen.
- 2 Since the residual stresses are produced at the damaged layer, their effects on the fatigue life are ignored.
- 3 The size effect is not considered, because the thickness of the damaged layer is small.
- 4 The crack growth is determined primarily by both the levels of the actual stress and the electrical pulse-induced damage.

This study used the stress life fatigue modeling analysis by using the ANSYS software 15.0. The cyclic fatigue of the material was obtained from completely reversed, constant amplitude tests with a load ratio of  $-1$  at room temperature. The Goodman mean stress correction theory is a good choice for hard materials. The flat bending workpieces were used for the fatigue test. The test frequency of the machine was maintained constant at 60 Hz. All the fatigue limits were defined at the stress level of 106 loading cycles. The von Mises stress theory, which takes the sign of the largest absolute principal stress, will be used to compare against the experimental stress value.

The Multiphysics, static structural models domain loads, includes the environment temperature, the fixing supported and the loading force. The fatigue strength concentration factor ( $K_f$ ), which is equal to 1 and 0.72 for flat as received specimens and for PMEDM machining workpieces [29], respectively, was set. The experimen-

tal fatigue results after EDM and PMEDM machining are given in Table 11 for the two groups.

The three-dimensional meshed domain models for the workpiece, using the triangle surface meshed mapping technique where the element pattern shapes meshing, were created with more elements mapped toward the machined regions for better study. The total elements and nodes numbers for establishing S/N curve for the flat as received specimens are 134,280 and 195,027, respectively and for EDM and PMEDM machining workpieces specimens are 83,824 and 123,748, respectively.

The experimental average values of fatigue stress at  $10^6$  cycles and numerical fatigue safety factor values for group (2) are given in Table 12. The fatigue safety factor values were calculated at  $10^6$  cycles of the experimental result respect to the fatigue stress at  $10^6$  cycles of the as-received material, which is equal to 270 MPa. The percentage enhancement in the value of experimental fatigue stresses at  $10^6$  cycles using SiC mixed powder (group 2) is compared with using kerosene dielectric alone (group 1) as shown in Table 13.

The maximum fatigue life and safety factor obtained by the FEM and PMEDM with ANSYS solutions and simulations using the copper and graphite electrodes using the pulse current of 8 A and pulse on time of 40  $\mu$ s are given in Fig. 9. Each simulation model in this figure shows two models for each of input parameters of PMEDM sub-group. The right figures represent the numerical modeled fatigue safety factor. The figures in the left show the fatigue life models simulations with the values of fatigue stresses at  $10^6$  cycles obtained from

**Table 12**

The experimental average values of fatigue stress at  $10^6$  cycles and fatigue safety factor for group (2) PMEDM machining with SiC powder mixing.

Exp. no.	Type of electrode	Pulse on time $T_{on}$ ( $\mu$ s)	Pulse off time $T_{off}$ ( $\mu$ s)	Pulse current (A)	Fatigue stress at $10^6$ cycles (Mpa)	Fatigue safety factor experiment	Fatigue safety factor numeric	Error in numeric mode %
1.	Copper	120	40	8	257	0.95	0.97	+2.1
2.	Copper	120	40	22	240	0.89	0.85	-4.5
3.	Copper	40	14	8	247	0.92	0.91	-1.1
4.	Copper	40	14	22	227	0.84	0.78	-7.1
5.	Graphite	120	40	8	275	1.02	1.13	+10.8
6.	Graphite	120	40	22	256	0.95	0.96	+1.1
7.	Graphite	40	14	8	267	0.99	1.06	+7.1
8.	Graphite	40	14	22	248	0.92	0.91	-1.1

**Table 13**

The experimental values of fatigue stress at  $10^6$  cycles for EDM group (1) and PMEDM group (2).

Exp. no.	Type of electrode	Pulse on time $T_{on}$ ( $\mu$ s)	Pulse off time $T_{off}$ ( $\mu$ s)	Pulse current (A)	Experimental fatigue stress at $10^6$ cycles (Mpa)		Percentage enhancement in fatigue stress (%)
					Group (1)	Group (2)	
1.	Copper	120	40	8	240	257	+7.1
2.	Copper	120	40	22	225	240	+6.7
3.	Copper	40	14	8	227	247	+8.8
4.	Copper	40	14	22	215	227	+5.6
5.	Graphite	120	40	8	232	275	+17.7
6.	Graphite	120	40	22	203	256	+26.1
7.	Graphite	40	14	8	223	267	+19.7
8.	Graphite	40	14	22	207	248	+20.1

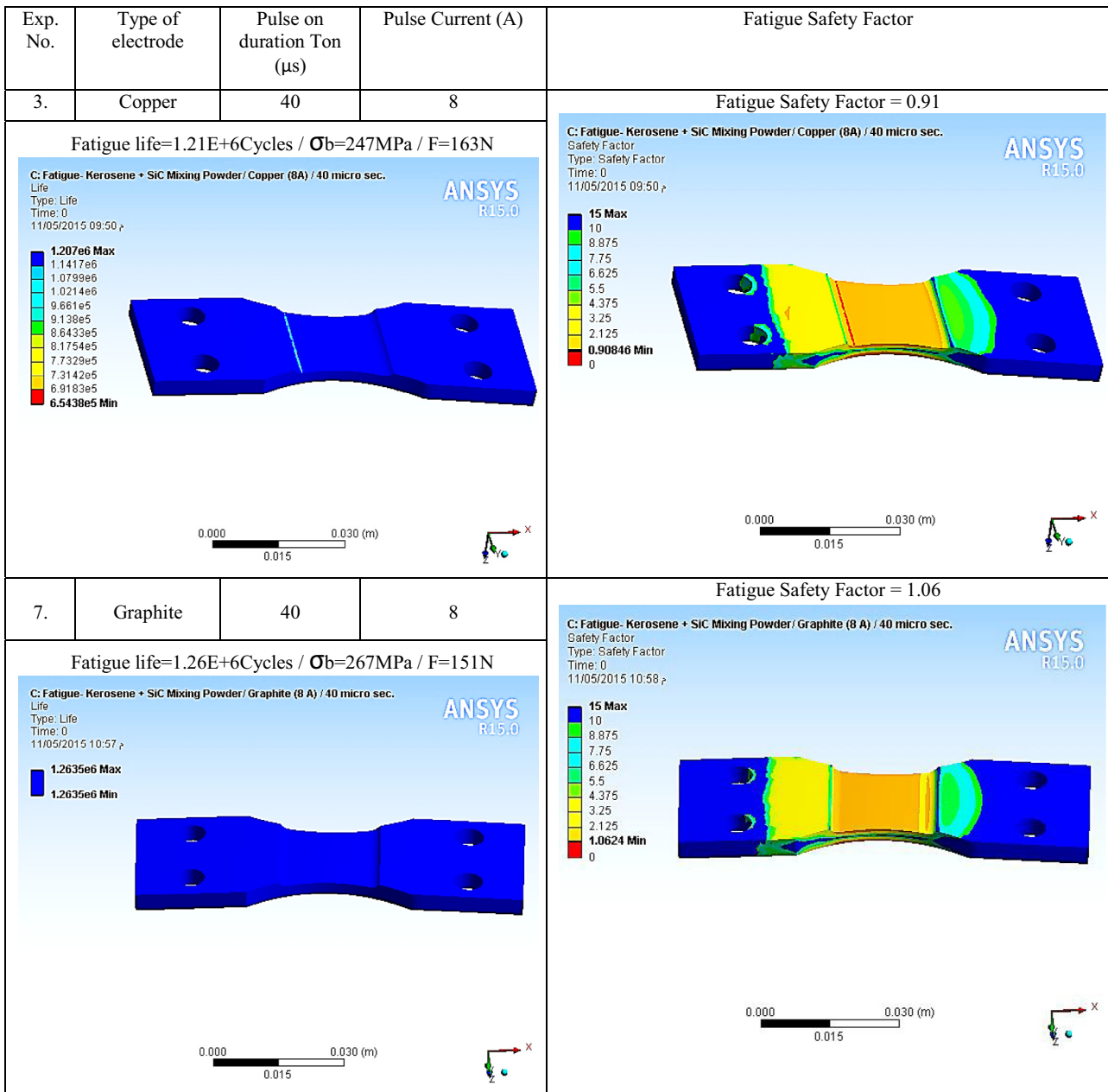


**Fig. 9.** The FEM Models for maximum fatigue life and safety factor of group (2) with SiC powder mixing (PMEDM) machining.

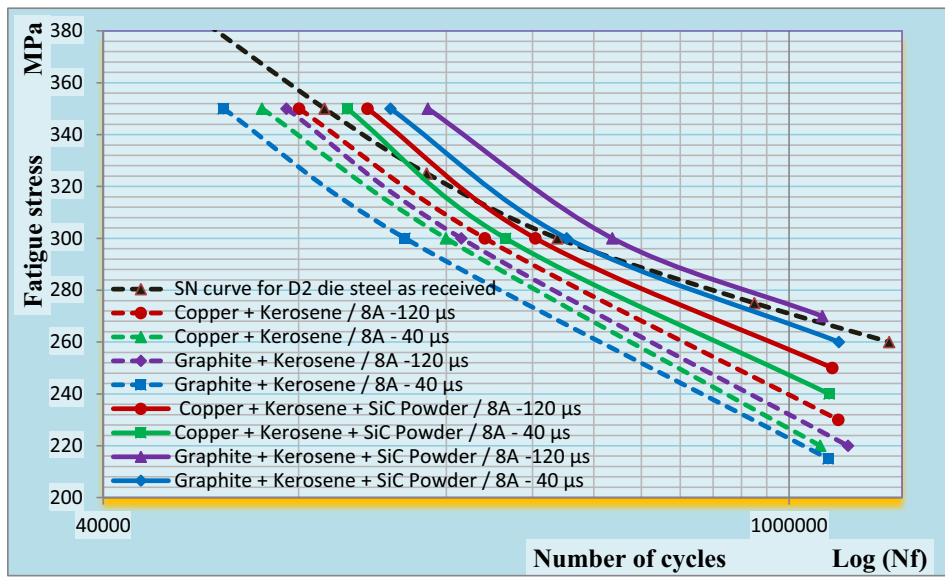


Fig. 10. The S/N curves of experimental groups (1) and (2) after EDM and PMEDM using the SiC powder mixing and pulse current (8 A).

the S/N curves of each experimental sub-group, the input EDM process parameters and the model loading force.

The S/N fatigue stress at  $10^6$  cycles curves for both groups after EDM and PMEDM machining is shown in Figs. 10 and 11 using pulse currents 8 A and 22 A, respectively. These figures show that fatigue life increasing with decreasing the pulse current and increasing the pulse on duration time, and copper electrodes gave fatigue life values higher than graphite electrodes, after EDM experimental group (1). Whereas, graphite electrodes gave fatigue life values higher than copper electrodes after PMEDM experimental group (2).

The three levels factorial response surface methodology (RSM) and the Design-Expert 9.0 software were used to analyze the obtained fatigue safety factor for each parametric subgroup.

The Model F-value of 444.81 implies that the model is significant. The “Pred R-Squared” of 0.9991 is in reasonable agreement

with the “Adj R-Squared” of 1.0000; i.e. the difference is less than 0.2.

The predicted equation of the fatigue safety factor for PMEDM experimental group (2) using kerosene dielectric with SiC mixing powder and copper electrodes is:

$$\text{Fatigue Safety Factor} = +0.96768 - 0.010179 * \text{Pulse current} + 7.81250 \text{E} - 004 * \text{Pulse on time (T}_{on}) \quad (9)$$

And, using graphite electrodes, the equation is:

$$\text{Fatigue Safety Factor} = +1.10518 - 0.010179 * \text{Pulse current} + 7.81250 \text{E} - 004 * \text{Pulse on time (T}_{on}) \quad (10)$$

The predicted equation of the fatigue stress at  $10^6$  cycles obtained by using copper electrodes is:

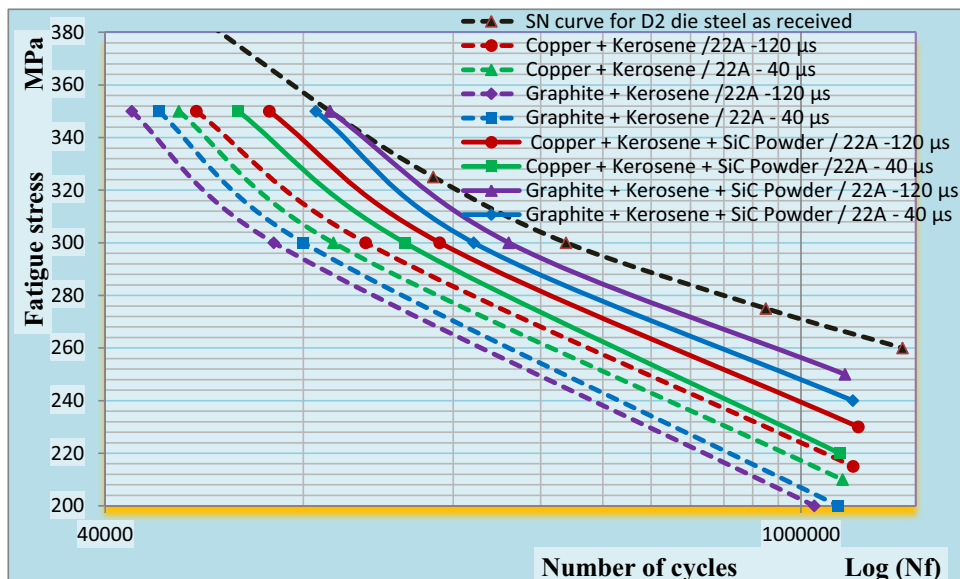


Fig. 11. The S/N curves for experimental groups (1) and (2) after EDM and PMEDM using the SiC powder mixing and pulse current (22 A).

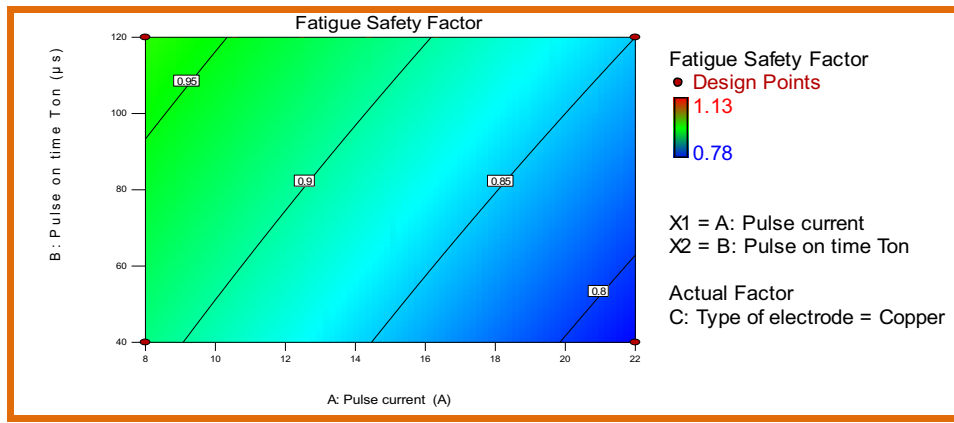


Fig. 12. The fatigue safety factor after EDM using copper electrodes and SiC mixed powder.

$$\begin{aligned} \text{Fatigue stress at 106 cycles} &= +253.08929 \\ &- 1.33929 * \text{Pulse current time} \\ &+ 0.12187 * \text{Pulse on time } (T_{on}) \end{aligned} \quad (11)$$

And, using graphite electrodes, the equation is:

$$\begin{aligned} \text{Fatigue stress at 106 cycles} &= +271.83929 \\ &- 1.33929 * \text{Pulse current time} \\ &+ 0.12187 * \text{Pulse on time } (T_{on}) \end{aligned} \quad (12)$$

The analysis of results for fatigue safety factor for experimental group (2) using the copper and graphite electrodes are shown in Figs. 12 and 13, respectively. While, the fatigue stresses at 106 cycles for all experimental groups using the copper and graphite electrodes are shown in Figs. 14 and 15, respectively.

The fatigue safety factor using the copper electrodes for experimental group (2) increases with the decrease in pulse current values and the increase in pulse on duration time, reaching its maximum value as 0.97, experimentally (0.95) at a current value of 8A and pulse time of 120 μs. While, when using the graphite electrodes, the fatigue safety factor values reached their maximum values as 1.13, experimentally (1.02) at the same input current and pulse on time period, as shown in Fig. 13.

This means that after PMEDM processes, the use of graphite electrodes and the kerosene dielectric with SiC mixed powder gives higher experimental fatigue safety factor values by 7.37%

compared with the use of copper electrodes and higher by 14.61% and 18.61% when compared with the results of group (1) using the copper and graphite electrodes, respectively.

The reason behind obtaining higher fatigue safety factor is because the use of low pulse current generates lower thermal energy, which cannot work to make a large metallurgical changes in the crystalline structure of the workpiece surface. Although the graphite electrode generates thermal energy more than that of copper, it works with the longer pulse time on annealing the workpiece surface and on reducing the creation of martensitic structure, assisted by the use of hard SiC particles powder that increases the removal rate of this layer by increasing erosive rates, and all that will lead to reducing the fatigue failure thereby increasing the fatigue life.

The fatigue stresses at 10<sup>6</sup> cycles after PMEDM experimental group (2) using the copper electrodes increase with the decrease in pulse current and the increase in pulse on duration time, reaching the maximum value as 257 MPa at a current value of 8 A and pulse on time 120 μs. Whereas, when using the graphite electrodes, these fatigue stresses values reached their maximum value as 275 MPa at the same input current and pulse on period time, i.e. improved by 7% as shown in Fig. 15.

This means that the use of graphite electrodes and the kerosene dielectric with SiC powder mixing yields higher fatigue stresses at 10<sup>6</sup> cycles values by 7.00% when compared with the use of copper electrodes and gives a higher fatigue life than the situation when working without mixing powder by 14.58% and 18.54% using the copper and graphite electrodes, respectively.

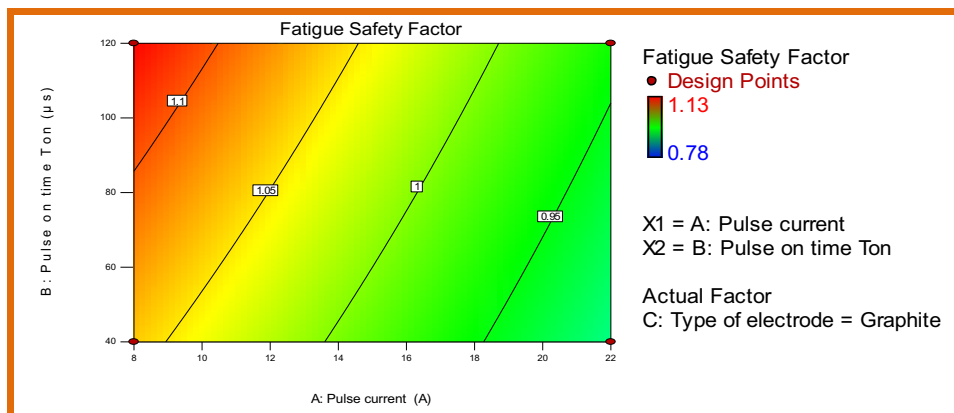


Fig. 13. The fatigue safety factor after EDM using graphite electrodes and SiC mixed powder.

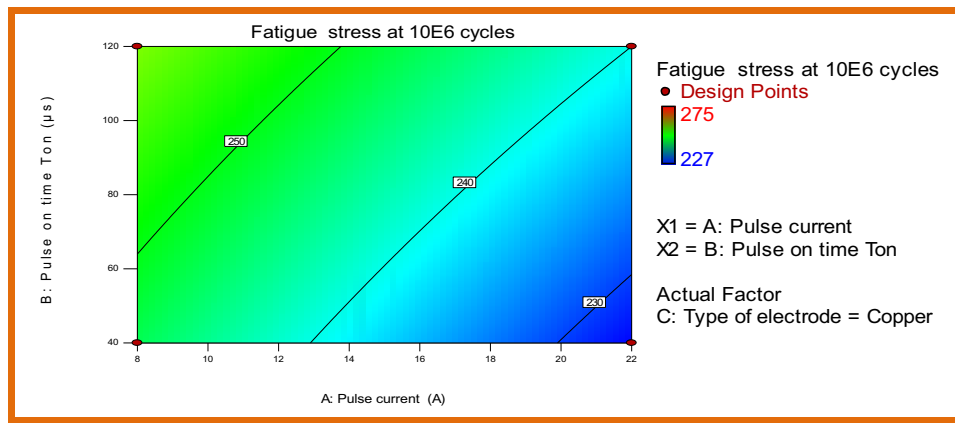


Fig. 14. The fatigue stresses at  $10^6$  cycles after EDM using copper electrodes and SiC mixed powder.

The stress values are equal to the ratios 0.95 and 1.02 for copper and graphite electrodes, respectively, compared with the fatigue stresses at  $10^6$  cycles for the as-received material.

Higher fatigue safety factor levels were obtained when using the copper electrodes with low current and high pulse on time period as lower heat discharges energy at the gap produced between the electrode and the workpiece. The longer time on period with the high abrasive effect of SiC powder work as micro shot peening of the machining surfaces, producing less brittle carbides formation, fewer defects and lower white layer thickness.

Also, the better surface roughness (SR) and white layer thickness (WLT) workpieces gave longer fatigue lives as less micro cracks and other surface defects were observed with less stress risers and stress concentration areas, helped eliminate the creation of cracks initiation and propagation, and then increased the dynamic service lives of the components.

And, all these factors are strengthening the workpiece against fatigue failure, and then longer lives were obtained.

**6. Conclusions**

- 1 The total heat flux values were increased with the increasing of pulse current values up to 22 A and the decreasing of pulse on duration time to 40 µs.
- 2 The graphite electrodes gave a total heat flux higher than copper electrodes by 82.4%, while using the SiC powder and graphite

electrodes gave a higher total heat flux than copper electrodes by 91.5%, and by 285.3% and 602.7% more than using the copper and graphite electrodes and the kerosene dielectric alone, respectively.

- 3 The lowest WLT values of 5.0 µm and 5.57 µm were reached at a high current and low current with low pulse on time using the copper and graphite electrodes and the SiC powder, respectively. This means that there is an improvement by 134% and 67% when compared with using the copper and graphite electrodes and kerosene dielectric alone, respectively.
- 4 The fatigue safety factor as compared with as-received material and fatigue stresses increased with the decrease of pulse current, and increase of pulse on time.
- 5 Using graphite electrodes with PMEDM and SiC powder yielded experimental fatigue safety factor values of 1.02, which is higher by 7.30% when compared with the use of copper electrodes and higher by 14.61% and 18.61% when compared with results of using the kerosene dielectric alone with copper and graphite electrodes, respectively.
- 6 The use of graphite electrodes with SiC powder gave fatigue stresses at  $10^6$  cycles as 275 MPa, which is higher by 7.00% when compared with the use of copper electrodes, and yielded a higher fatigue life than when working without mixing powder by 14.58% and 18.54% using the copper and graphite electrodes, respectively.
- 7 All predicted fatigue stresses to the fatigue stresses at  $10^6$  cycles for the as-received material ratio are close with those results of fatigue safety factors for the same input parameters, and this

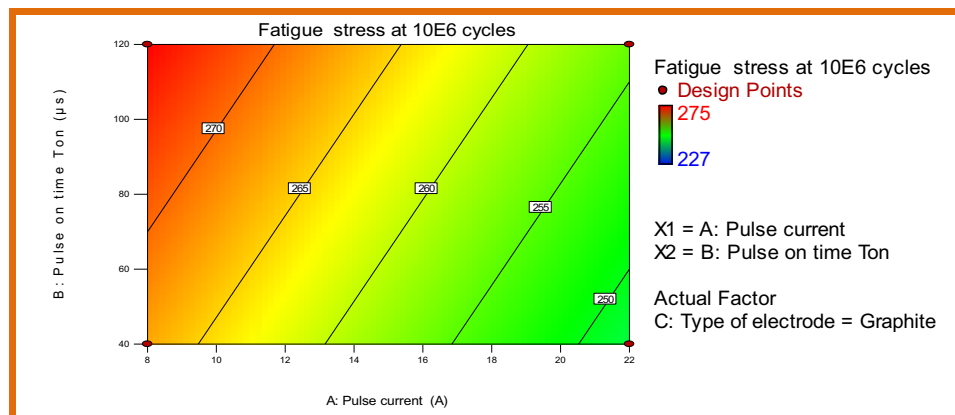


Fig. 15. The fatigue stresses at  $10^6$  cycles after EDM using graphite electrodes.

proves the accuracy of EDM and PMEDM models developed by FEM using ANSYS software.

## References

- [1] R. Atefi, N. Javam, A. Razmavar, F. Teimoori, The influence of EDM parameters in finishing stage on surface quality, MRR and EWR, Res. J. Appl. Sci. Eng. Technol. 4 (10) (2012) 1287–1294.
- [2] S. Prabhu, B.K. Vinayagam, Analysis of surface characteristics of AISI D2 tool steel material using Electric Discharge Machining process with Single wall carbon nano tubes, Int. J. Eng. Technol. 2 (2010) 35–41.
- [3] N.S. Khundrakpam, H. Singh, S. Kumar, G.S. Brar, Investigation and modeling of silicon powder mixed EDM using response surface method, Int. J. Curr. Eng. Technol. 4 (2) (2014) 1022–1026.
- [4] M.A. Razak, A.M. Abdul-Rani, A.M. Nanimina, Improving EDM efficiency with silicon carbide powder-mixed dielectric fluid, Int. J. Mater. Mech. Manuf. 3 (1) (2015) 40–43.
- [5] B. Reddy, G.N. Kumar, K. Chandrashekar, Experimental investigation on process performance of powder mixed electric discharge machining of AISI D3 steel and EN-31 steel, Int. J. Curr. Eng. Technol. 4 (3) (2014) 1218–1222.
- [6] V.M. Abhijeetsinh, S.B. Kapil, An experimental investigation on AISI 316 stainless steel for tool profile change in die sinking EDM using DOE, Sch. J. Eng. Technol. 3 (4B) (2015) 447–462.
- [7] H. Singh, Experimental study of distribution of energy during EDM process for utilization in thermal models, Int. J. Heat Mass Transf. 55 (2012) 5053–5064.
- [8] B. Izquierdo, J.A. Sanchez, S. Plaza, I. Pombo, N. Ortega, A numerical model of the EDM process considering the effect of multiple discharges, Int. J. Mach. Tools Manuf. 49 (3–4) (2009) 220–229.
- [9] H. Mehdi, F. Saeed, A.A. Sarhan, Y.N. Mohd, Investigating the electrical discharge machining (EDM) parameter effects on Al-Mg2Si metal matrix composite (MMC) for high material removal rate (MRR) and less EWR-RSM approach, Int. J. Adv. Manuf. Technol. 77 (5) (2015) 831–838.
- [10] P.N. Santoki, P.B. Ashwin, A review – status of recent developments and effect of machining parameters on performance parameters in EDM, Int. J. Innov. Emerg. Res. Eng. 2 (1) (2015) 32–41.
- [11] K.J. Sabareesaan, R. Varahamoorthi, A. Habeeb Al, J. Jaya, MRR prediction model for electrical discharge machining of INCONEL X750 by response surface methodology using MINITAB software, Eur. J. Adv. Eng. Technol. 2 (2) (2015) 29–33.
- [12] S. Vikram, S.K. Pradhan, Optimization of EDM process parameters: a review, Int. J. Emerg. Technol. Adv. Eng. 4 (3) (2014) 345–355.
- [13] S. Hirendra, Jasdeep, optimization of dry EDM by using super alloy: a review, Int. J. Technol. Innov. Res., Vol. XY (2014) 1–9.
- [14] J. Jeevamalar, S. Ramabalan, Die sinking EDM process parameters: a review, Int. J. Mech. Eng. Rob. Res. (2015) 315–326.
- [15] M.K. Pradhan, C.K. Biswas, Predictive modeling and analysis of surface roughness in electro-discharge machining of D2 tool steel using regression and neural networks approach, Int. J. Design Manuf. Technol. 3 (2009) 20–29.
- [16] ASTM A370, Standard Test Method and Definitions for Mechanical Testing of Steel Products, American Society for Testing and Materials, Washington, DC, 1977.
- [17] ASTM A681, Standard Specification for Tool Steels Alloy, American Society for Testing and Materials, Washington, DC, 1976.
- [18] V. Yadav, V.K. Jain, P.M. Dixit, Thermal stresses due to electrical discharge machining, Int. J. Mach. Tools Manuf. 42 (2002) 877–888.
- [19] D. Shuvra, K. Mathias, F. Klocke, EDM simulation: finite element-based calculation of deformation, microstructure and residual stresses, J. Mater. Process. Technol. 142 (2003) 434–451.
- [20] D.D. Dibitonto, P.T. Eubank, M.R. Patel, M.A. Barrufet, Theoretical models of the electrical discharge machining process. I. A simple cathode erosion model, J. Appl. Phys. 66 (1989) 4095–4103.
- [21] M.R. Patel, M.A. Barrufet, P.T. Eubank, D.D. Dibitonto, Theoretical models of the electrical discharge machining process. II the anode erosion model, J. Appl. Phys. 66 (1989) 4104–4111.
- [22] P. Shankar, V.K. Jain, T. Sundarajan, Analysis of spark profiles during EDM process, Mach. Sci. Technol. 1 (2) (1997) 195–217.
- [23] A. Erden, B. Kaftanoglu, Heat transfer modeling of electric discharge machining, in: 21st MTDR Conference, Swansea, 1980, pp. 351–358.
- [24] S.T. Jilani, P.C. Pandey, Analysis and modeling of EDM parameters, Precis. Eng. 4 (4) (1982) 215–221.
- [25] P.E. Eubank, M.R. Patel, M.A. Barrufet, B. Bozkurt, Theoretical models of the electrical discharge machining process III. The variable mass, cylindrical plasma model, J. Appl. Phys. 73 (11) (1993) 7900–7909.
- [26] R. Bhattacharya, V.K. Jain, P.S. Ghoshdastidar, Numerical simulation of thermal erosion in EDM process, IE (1) J.-PR 77 (1996) 13–19.
- [27] J. Marafona, J.A. Chousal, A finite element model of EDM based on the Joule effect, Int. J. Mach. Tools Manuf. 46 (2006) 595–602.
- [28] B. Raymond, A. Hancq, Calculating and Displaying Fatigue Results – The ANSYS Fatigue Module, New Technologies, ANSYS, Inc., 2006.
- [29] J.E. Shigley, C.R. Mischke, Mechanical Engineering Design, 8th ed., McGraw-Hill Inc., 2006, pp. 1007–1014.